Hindawi
Mathematical Problems in Engineering
Volume 2023, Article ID 9911612, 11 pages
https://doi.org/10.1155/2023/9911612

Research Article

Finite Element and Vibration Frequency Analysis of Cracked Solid Beams: A Comparison of Iron, Steel, and Titanium Materials

Rajib Karmaker [1,2] **and Ujjwal Kumar Deb** [2]

[1]*Department of Mathematics, University of Chittagong, Chattogram 4331, Bangladesh*
[2]*Department of Mathematics, Chittagong University of Engineering and Technology, Chattogram 4349, Bangladesh*

Correspondence should be addressed to Rajib Karmaker; rajibcumath@gmail.com

Received 3 July 2023; Revised 14 October 2023; Accepted 24 October 2023; Published 21 November 2023

Academic Editor: Salvatore Caddemi

Different solid materials are widely used in various constructions due to their availability and low cost. However, cracks or conversions in the structures can affect their stiffness and vibration signatures. This research aims to evaluate the load distribution, deformation, and the effects of the cracks on the natural frequencies and deformations of iron, steel, and titanium beams. A finite element-based model and COMSOL Multiphysics software were employed to measure and compare the frequencies and strengths of the beams. The results showed that the frequencies increased with the load, and titanium beams had the highest frequencies and deflections, while steel beams had the highest stress resistance. This frequency analysis can help to detect very small cracks (less than 0.05 mm) in the beams. The study concluded that steel is the most suitable material for construction due to its elasticity, availability, and low cost.

1. Introduction

Structural health monitoring and failure detection are important research topics in engineering [1]. Many civil structures and constructions around the world may suffer damage during their service life, which can endanger human lives [2]. Cracking is a common damage indicator that can reduce the stress capacity and stability of the structures. Therefore, detecting and analyzing cracks are essential for structural safety [3]. One way to detect cracks is to use vibration-based methods, which measure how cracks affect the local stiffness, natural frequency, and mode shape of the structures [4]. Many researchers have used different models and methods to study cracks in the various structures. Some of their findings are summarized as follows: Patil and Maiti [5] used frequency measurement to detect multiple cracks in a beam. They showed how frequency depends on crack size and location. Darpe et al. [6] studied a cracked rotor under surface loading. They found that the crack did not change the vibration direction, but it changed the rotation speed. Chasalevris and Papadopoulos [7] studied multiple cracks in beams under bending. They used a matrix method to model how each crack affects the beam's motion. They could determine the size, depth, and location of each crack. Darpe [8] studied a side crack in a rod under bending and friction. He found that the crack changed the rod's vibration pattern. Prabhakar [9] studied a beam with two side cracks using vibration analysis. He used matrix methods to model the cracks based on their size and location. He found that the cracks changed the beam's stiffness and vibration mode. Dackermann [10] used dynamic fingerprints and artificial intelligence to identify defects in structures. He trained his system to recognize different types of damage using vibration data. Georgantzinos and Anifantis [11] studied a crack in a cylindrical beam with different shapes. They found that the shape of the crack affected its opening and closing behavior. Shahbazpanahi and Kamgar [12] modeled crack growth in steel using an interface element with springs that can soften or harden. He used VCCT to estimate the energy release rates and applied fracture criteria to analyze crack growth. Caliò et al. [13] studied the vibration frequencies of spatial arches with and without damage. He compared different parameters and showed how some results can be misleading for inverse problem solutions. Jirásek [14] proposed an isotropic damage model that uses two scalar

variables for the damaged stiffness tensor, based on the initial elastic stiffness tensor and the standard isotropic elasticity constants. Cervera and chiumenti [15] reviewed the discrete and smeared crack approaches for tensile cracking problems in the last 40 years. He focused on the smeared approach and pointed out its main limitations, such as the mesh-size and mesh-bias dependence.

This paper aims to simulate and compare the vibration and deformation behavior of uncracked and cracked cylindrical iron, steel, and titanium beams with half-open micro cracks. It also analyses the relationship between the modal natural frequencies and different crack positions for different materials (iron, steel and titanium) based on vibration analysis by using simulation.

2. Mathematical Modeling

Vibration-based methods are popular for crack detection in the structures, because they are effective and reliable [16]. This method depends on how the physical responses, such as natural frequency and crack placement criterion, change [17]. A solid cylindrical beam of iron, steel, and titanium with a crack in its body is considered. Bending deformations involve changes in shape and curvature of the structure, which depend on the transversal displacements and bending stiffness. Transversal displacements are the movements perpendicular to the direction of the applied force, and bending stiffness is a measure of how much resistance a structure offers to bending. The governing equation system for the deformation can be written as follows [18]:

$$\mathrm{EI}\frac{d^4r(x)}{dx^4} + q(x) = 0, \tag{1}$$

where

$q(x) = cx =$ Transmitted load (c = constant)

$I =$ Second moment of area

$E =$ Young's Modulus

$r(x) =$ Transversal displacement

Since the domain is free on both ends, so the boundary condition will be: $\boldsymbol{r}(\boldsymbol{x_0}) = \mathbf{0}$, $\boldsymbol{r}(\boldsymbol{x_L}) = \mathbf{0}$, and $\left|\frac{\boldsymbol{dr(x)}}{\boldsymbol{dx}}\right|_{\boldsymbol{x=L=0}}$

This equation relates the bending moment and the curvature of the beam as follows:

$$M = -\mathrm{EI}\frac{d^2r(x)}{dx^2}. \tag{2}$$

Strain energy is the energy stored by a deformed material or structure due to external loads. A crack creates a high stress field near its tip, where the strain energy concentrates. The stress intensity factor, K, measures this stress field and depends on the crack geometry, the applied load, and the loading mode [19]. The strain energy release rate at the cracked section is,

$$E_S = \frac{\mathbf{1}}{E}(K_{I\mathbf{1}} + K_{I\mathbf{2}})^{\mathbf{2}}, \tag{3}$$

where the stress intensity factors are K_{I1}, K_{I2} of Mode I (opening of the crack) under load P_1 and P_2, respectively.

There are three loading modes: Mode I (opening mode), Mode II (sliding mode), and Mode III (tearing mode). For a Mode I crack, the stress intensity factor can be written as follows:

$$K_I = \sigma\sqrt{\pi a}, \tag{4}$$

where σ is the applied stress, and a is the crack length. The strain energy release rate, G, is a measure of the energy available for crack growth per unit increase in crack area. For a mode I crack, G can be related to K_I by:

$$G = \frac{K_I^2}{\acute{E}}, \tag{5}$$

where $\acute{E}$ is an effective modulus that depends on the material's Young's modulus, E, and Poisson's ratio, ν. For plane stress conditions, $\acute{E} = \frac{E}{1-\nu^2}$ and for plane strain conditions, $\acute{E} = E$.

Now, suppose we have a cracked body under two different loads, P_1 and P_2, that produce two different stress intensity factors, K_{I1} and K_{I2}, respectively. The total strain energy stored in the body can be written as follows:

$$U = U_0 + U_1 + U_2, \tag{6}$$

where U_0 is the strain energy without load or crack, U_1 is the strain energy due to load P_1, and U_2 is the strain energy due to load P_2. U_0 is negligible compared to the other terms. The loads are applied independently and do not interact. Hence, the equation is:

$$U_1 = \frac{1}{2}P_1\delta_1,\ U_2 = \frac{1}{2}P_2\delta_2, \tag{7}$$

where δ_1 and δ_2 are the displacements at the crack tip due to loads P_1 and P_2, respectively. Using Castigliano's theorem, these displacements can be express as follows:

$$\begin{aligned}\delta_1 &= \frac{\partial U}{\partial P_1} = \frac{\partial U_1}{\partial P_1} + \frac{\partial U_2}{\partial P_1} = \frac{1}{2}\frac{\partial P_1^2}{\partial P_1}\frac{\partial U_1}{\partial P_1^2} + \frac{1}{2}\frac{\partial P_2^2}{\partial P_1}\frac{\partial U_2}{\partial P_2^2} \\ &= P_1\frac{\partial U_1}{\partial P_1^2} + 0 = P_1\frac{\partial U_1}{\partial K_{I1}^2}\frac{\partial K_{I1}^2}{\partial P_1^2},\ \delta_2 = \frac{\partial U}{\partial P_2} = \frac{\partial U_1}{\partial P_2} + \frac{\partial U_2}{\partial P_2} \\ &= \frac{1}{2}\frac{\partial P_1^2}{\partial P_2}\frac{\partial U_1}{\partial P_1^2} + \frac{1}{2}\frac{\partial P_2^2}{\partial P_2}\frac{\partial U_2}{\partial P_2^2} = 0 + P_2\frac{\partial U_2}{\partial P_2^2} = P_2\frac{\partial U_2}{\partial K_{I2}^2}\frac{\partial K_{I2}^2}{\partial P_2^2}.\end{aligned} \tag{8}$$

The expression for stress intensity factors from earlier studies of Irwin et al. [3] are,

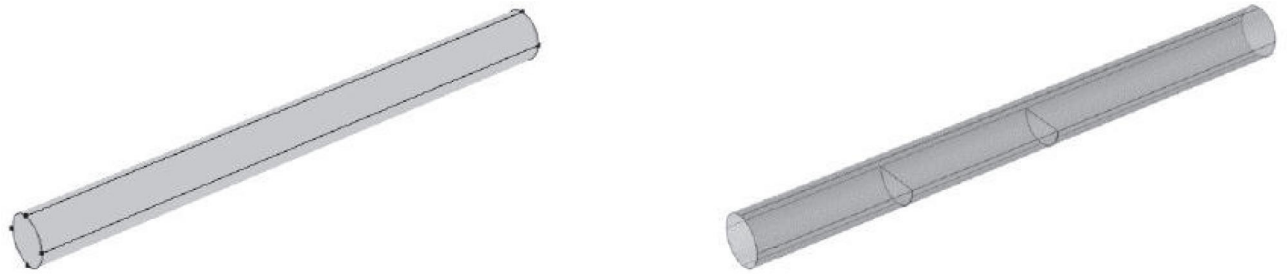

Figure 1: Computational domain with crack.

$$K_{I1} = \frac{P_1}{WH}\sqrt{\pi h}\left(F_1\left(\frac{h}{H}\right)\right) \text{ and } K_{I2} = \frac{6P_2}{WH^2}\sqrt{\pi h}\left(F_2\left(\frac{h}{H}\right)\right). \tag{9}$$

Here, W = width of the domain containing the crack
H = height of the domain containing the crack
h = distance from the crack tip to the free surface of the domain
F_1 and F_2 are applied forces acting on the crack edges
Defining the flexibility influence coefficient C_{ij} per unit depth [20],

$$C_{ij} = \frac{\delta r_i}{\delta P_j} = \frac{\delta^2 r_i}{\delta P_i \delta P_j}\int_{-W/2}^{W/2}\int_0^h J_C(h)\,dh\,dz, \tag{10}$$

where U_c represents the strain energy of the considered domain and $J_C = \frac{\delta U_C}{\delta h}$ is strain energy release rate. So that,

$$r_i = \frac{\delta}{\delta P_i}\left[\int_0^{n_1} J_C(h)\,dh\right]. \tag{11}$$

Using the stress intensity rate (J_C), it is found that,

$$C_{ij} = \frac{B}{\dot{E}}\frac{\delta^2}{\delta P_i \delta P_i}\int_0^{h_1}(K_{I1} + K_{I2})^2\,dh. \tag{12}$$

Here, $\dot{E}$ is the crack growth rate, which is the change of crack length per unit time. The local stiffness matrix can be obtained by taking inverse of compliance matrix [18],

$$[K] = \begin{bmatrix} K_{11} & K_{12} \\ K_{21} & K_{22} \end{bmatrix} = \begin{bmatrix} C_{11} & C_{12} \\ C_{21} & C_{22} \end{bmatrix}^{-1} \tag{13}$$

The stiffness matrix to detect first crack is,

$$[K'] = \begin{bmatrix} C'_{11} & C'_{12} \\ C'_{21} & C'_{22} \end{bmatrix} \tag{14}$$

The stiffness matrix to detect second crack is,

$$[K''] = \begin{bmatrix} C''_{11} & C''_{12} \\ C''_{21} & C''_{22} \end{bmatrix}^{-1} \tag{15}$$

In this study a solid cylindrical beam of iron, steel, or titanium with a length of 0.60 m and a radius of 0.015 m has been considered as the domain as shown in Figure 1. Figure 2 represents the mesh design and Figure 3 represents the internal computational geometry of the domain for the uncracked and cracked beams, which were created using COMSOL Multiphysics software [21]. Tables 1 and 2 enlisted the properties of the mesh for the domain.

3. Results and Discussion

Stress analysis can be used to explain how bodies can deform and fracture as well as find cracks [22]. The frequency and load distribution of iron, steel, and titanium beams with half circular double cracks have been studied using the finite element method. A solid cylindrical iron, steel, or titanium beams were modeled using a number of the parameters listed in Tables 3 and 4.

Figure 4 shows how a load of 500 N is applied on the edge of the beam's crown. Figure 5 illustrates the deformation of the body after the load is applied, which is simulated using COMSOL Multiphysics.

Figure 6 shows the pattern of stress distribution in the entire domain for all materials. The stress is maximum at the crack location for all metals, as shown in Figure 6(a)–6(i). The iron, steel, and titanium beams that are not cracked transfer the weight evenly to the end of the body, as shown in Figure 6(j)–6(l). No matter where the crack was, the titanium body flexed more than any other body.

Figure 7 shows how the load is distributed in a cross-section of iron, steel, and titanium beams. The load is highest at the crack location for all metals, as seen in Figure 7(a)–7(i). Iron and titanium beams have more stress at the crack location than steel beams, which have a uniform stress distribution in the body. The uncracked beams have a constant stress on the top edge of the domain, as seen in Figure 7(j)–7(l).

Figure 8 illustrates the stress absorption at various crack positions (0.01 and 0.10 m from the first end of the beam). The steel beam, which bends the most, pass the load to the

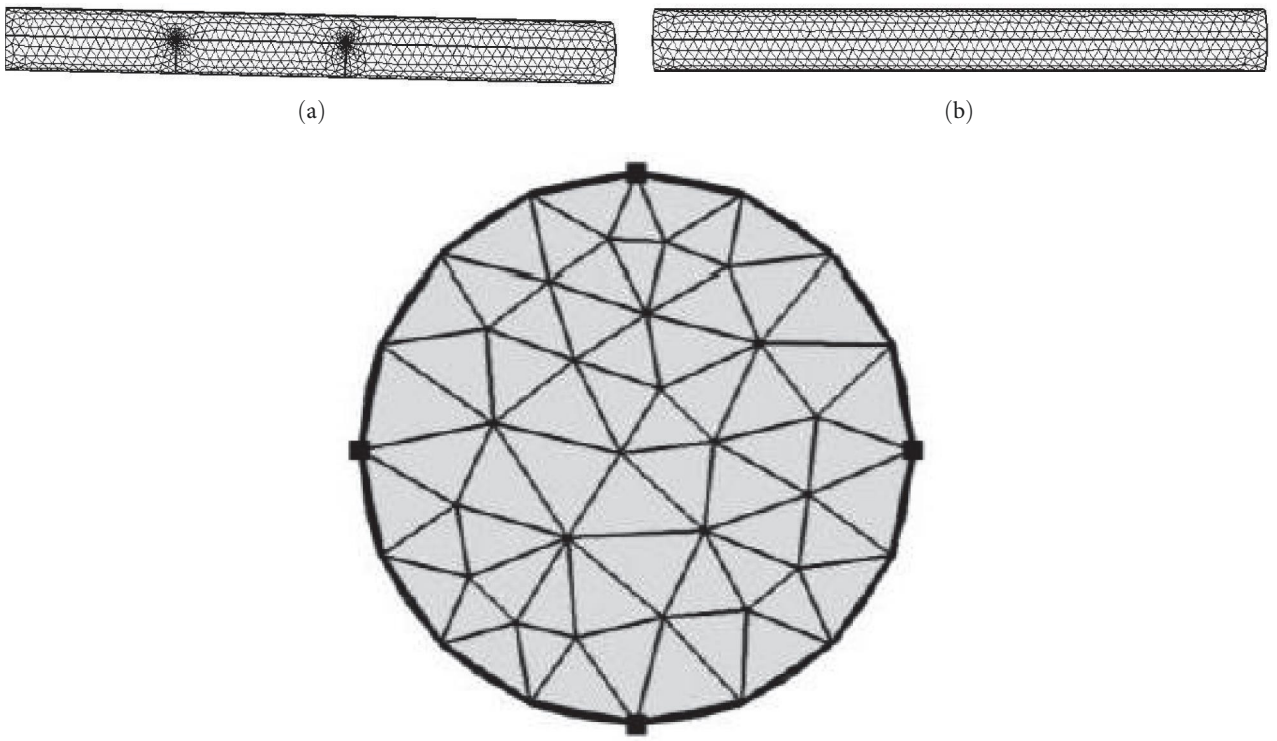

(a) (b) (c)

Figure 2: Mesh design of computational domain. (a) Along the cracked beam. (b) Along the uncracked beam. (c) Inlet of the beam.

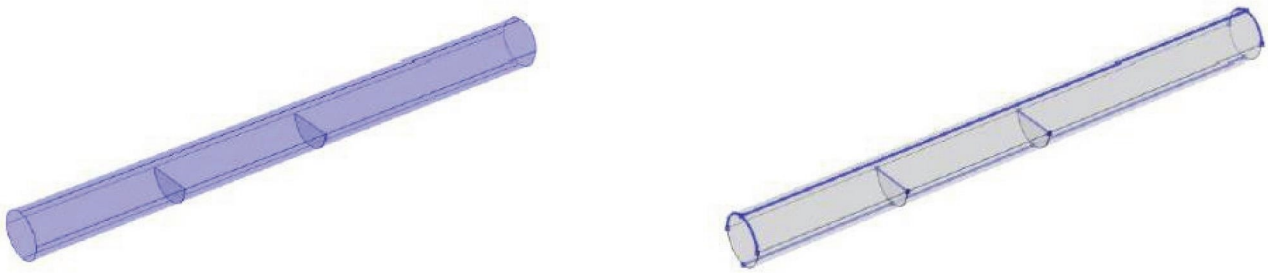

Figure 3: Internal geometry of the domain.

Table 1: Mesh properties of the domain.

Description	Value	Description	Value
Minimum element quality	0.1316	Maximum element size	0.022
Average element quality	0.6592	Minimum element size	0.0016
Tetrahedron	17,412	Curvature factor	0.4
Triangle	4,192	Resolution of narrow regions	0.7
Edge element	507	Maximum element growth rate	1.4
Vertex element	20	Predefined size	Finer

Table 2: Geometrical properties of computational domain.

Description	Value	Description	Value
Number of degrees of freedom	17,587	Strain reference temperature	293.15 K
Spatial dimension	3	Number of boundary elements	3,976
Number of domains	1	Number of elements	17,163
Number of boundaries	16	Number of vertex elements	20
Number of edges	34	Number of edge elements	485

Table 3: Properties of computational domain.

Description	Value
Length of the beam (L)	0.60 m
Radius of the beam (r)	0.015 m
Width of First crack ($c_1 l$)	0.00027 m
Depth of First crack ($c_1 h$)	0.03 m
Width of second crack ($c_2 l$)	0.00027 m
Depth of second crack ($c_2 h$)	0.03 m

Table 4: Properties of materials.

Properties	Iron	Steel	Titanium	Unit
Density	7,870	7,850	4,430	kg/m³
Young's modulus	200	200	113.8	GPa
Poisson's ratio	0.29	0.30	0.34	1
Shear modulus	5.5 E9	73.3 E9	36 E9	N/m^2
Tensile Strength	540	430	240	MPa
Heat capacity at constant pressure	440	475	520	J/(kg*K)
Relative permeability	4,000	1	1.0001	1
Electrical conductivity	1.12 E7	4.032 E6	3.28 E6	S/m
Thermal conductivity	76.2	44.5	24.5	W/(m*K)

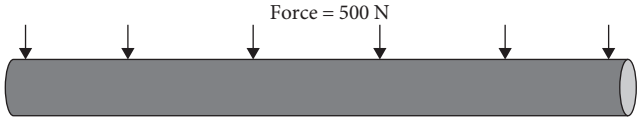

Figure 4: Applying force on the apex of computational domain.

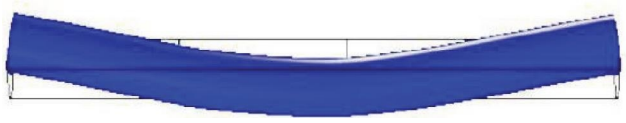

Figure 5: Deformation of the domain after applying load.

lower part of the crack and disperses it evenly to the edge of the domain. The iron and titanium beams act in a similar way, but they do not distribute the load as evenly as steel does throughout the whole body.

Figure 9 shows the load absorption nearer to crack positions (at 0.0085 and 0.085 m) from the beam's starting end. The bottom of the domain receives the most stress. The load was applied at the top edge of the domain, but as it moved to the bottom edge, it created significant, periodic vibration, particularly where the crack existed.

Figure 10 shows the relationship between the frequency of iron, steel, and titanium beams and the load, for a constant crack position. Iron has a higher frequency than steel and titanium for any load, because iron takes more load at the crack location (at 0.01 and 0.10 m from starting point), resulting in more vibration. As the load increases, each beam's frequency curve rises because the stress distribution does as well. This means that when a load is applied to a cracked body, iron is more likely to endure fracture than steel or titanium.

Figure 11 illustrates the deflection of different materials (iron, steel, and titanium) at the crack location and also for intact beam under stress. Titanium bends the most among all materials for both cracked and uncracked cases. Iron and steel have almost the same deflection and load absorption for uncracked cases. However, titanium takes too much stress at the crack location.

Figure 12 displays the deflection of three different materials (iron, steel, and titanium) without any cracks. The graph shows how the deflection of the materials changes at different locations along the body's length, from 0 to 0.3 m. The graph indicates that titanium bends the most, followed by steel and then iron. The graph also indicates that the deflection is not consistent and differs depending on the location.

The deflection of three different materials (iron, steel, and titanium) with cracks at 0.10 m positions is displayed in Figure 13. The graph demonstrates how the deflection of the materials varies at different locations along the length of the body, from 0 to 0.3 m. The graph reveals that steel has the most bending, followed by iron and then titanium. The graph also reveals that the bending is greatest at the positions where the cracks are, which are 0.10 and 0.20 m from the first end of the domain.

4. Conclusions

This study used a finite element-based model and COMSOL Multiphysics software to simulate the effects of cracks on the natural frequencies, deflections, and stresses of the solid cylindrical beams made of iron, steel, and titanium. The

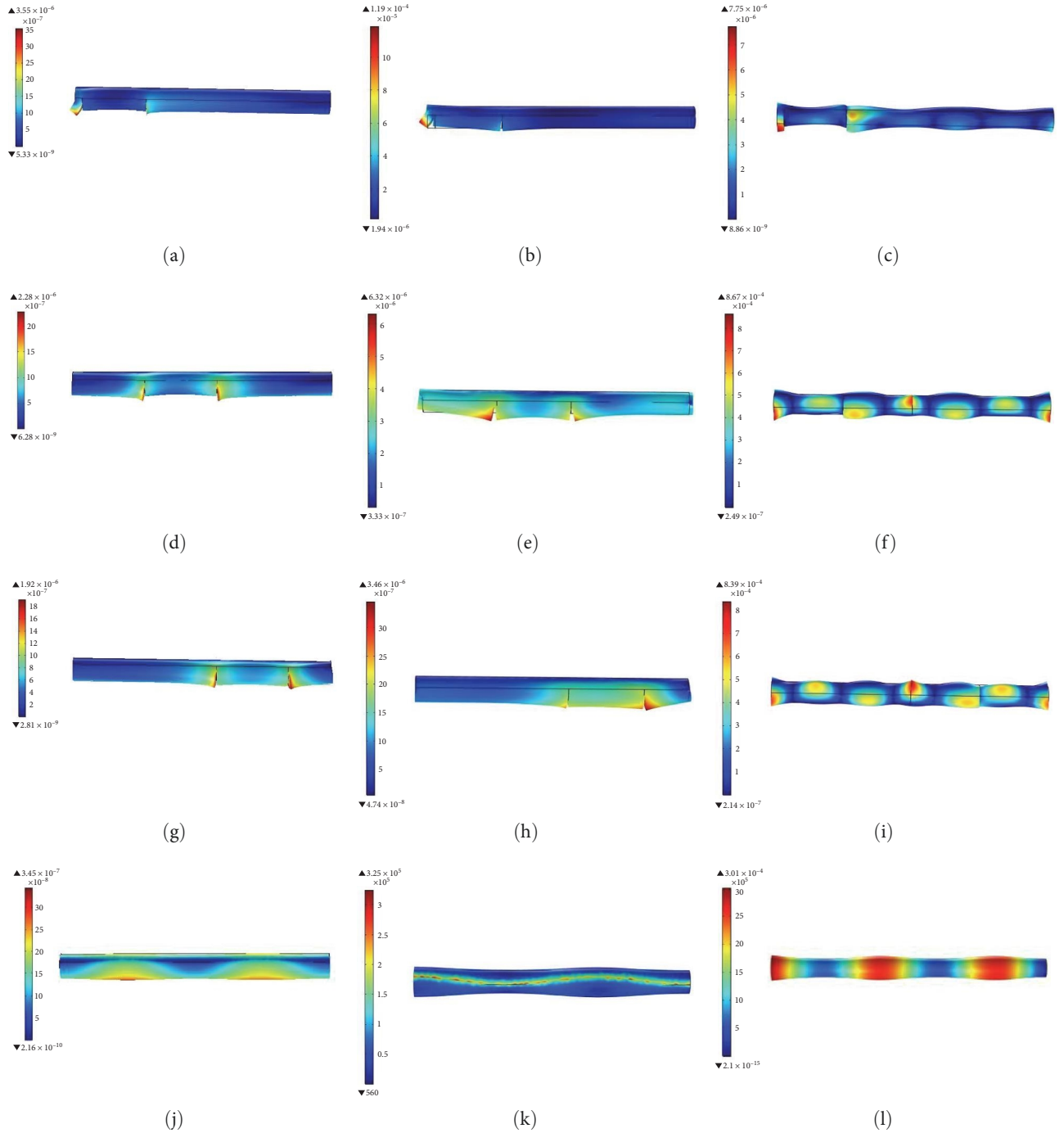

Figure 6: Phase of the stress absorbance at different crack position. (a) Position of first crack at 0.01 m and second crack at 0.10 m of iron. (b) Position of first crack at 0.01 m and second crack at 0.10 m of steel. (c) Position of first crack at 0.01 m and second crack at 0.10 m of titanium. (d) Position of first crack at 0.10 m and second crack at 0.20 m of iron. (e) Position of first crack at 0.10 m and second crack at 0.20 m of steel. (f) Position of first crack at 0.10 m and second crack at 0.20 m of titanium. (g) Position of first crack at 0.20 m and second crack at 0.30 m of iron. (h) Position of first crack at 0.20 m and second crack at 0.30 m of steel. (i) Position of first crack at 0.20 m and second crack at 0.30 m of titanium. (j) Uncracked iron beam. (k) Uncracked steel beam. (l) Uncracked titanium beam.

study focuses on method for crack detection using vibration analysis, based on the assumption that cracks affect the frequency and strength of the beams. The results showed that the material, size, and position of the cracks influenced the dynamic behavior of the beams. Steel beams had lower deflection and higher stress resistance than iron and titanium beams, while titanium beams had higher frequencies and deflections than iron and steel beams. The analysis was able to detect very small cracks (less than 0.05 mm) in the beams. These results suggest that steel is the best material for construction because of its elasticity, availability, and low cost. This study contributes to the field of structural health

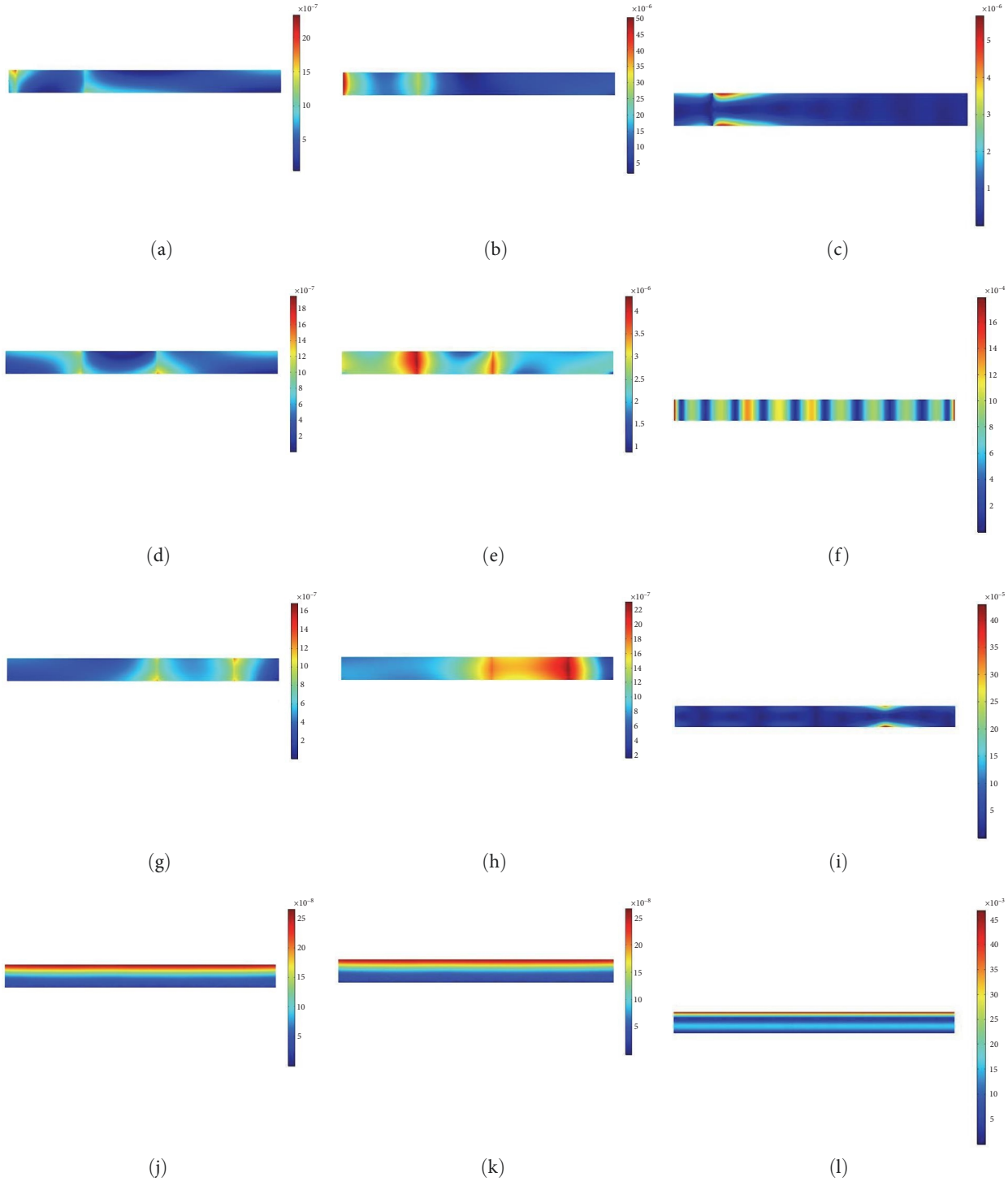

Figure 7: Slice of the cross-section of load distributions for iron, steel and titanium bodies. (a) Position of first crack at 0.01 m and second crack at 0.10 m of iron. (b) Position of first crack at 0.01 m and second crack at 0.10 m of steel. (c) Position of first crack at 0.01 m and second crack at 0.10 m of titanium. (d) Position of first crack at 0.10 m and second crack at 0.20 m of iron. (e) Position of first crack at 0.10 m and second crack at 0.20 m of steel. (f) Position of first crack at 0.10 m and second crack at 0.20 m of titanium. (g) Position of first crack at 0.20 m and second crack at 0.30 m of iron. (h) Position of first crack at 0.20 m and second crack at 0.30 m of steel. (i) Position of first crack at 0.20 m and second crack at 0.30 m of titanium. (j) Uncracked iron beam. (k) Uncracked steel beam. (l) Uncracked titanium beam.

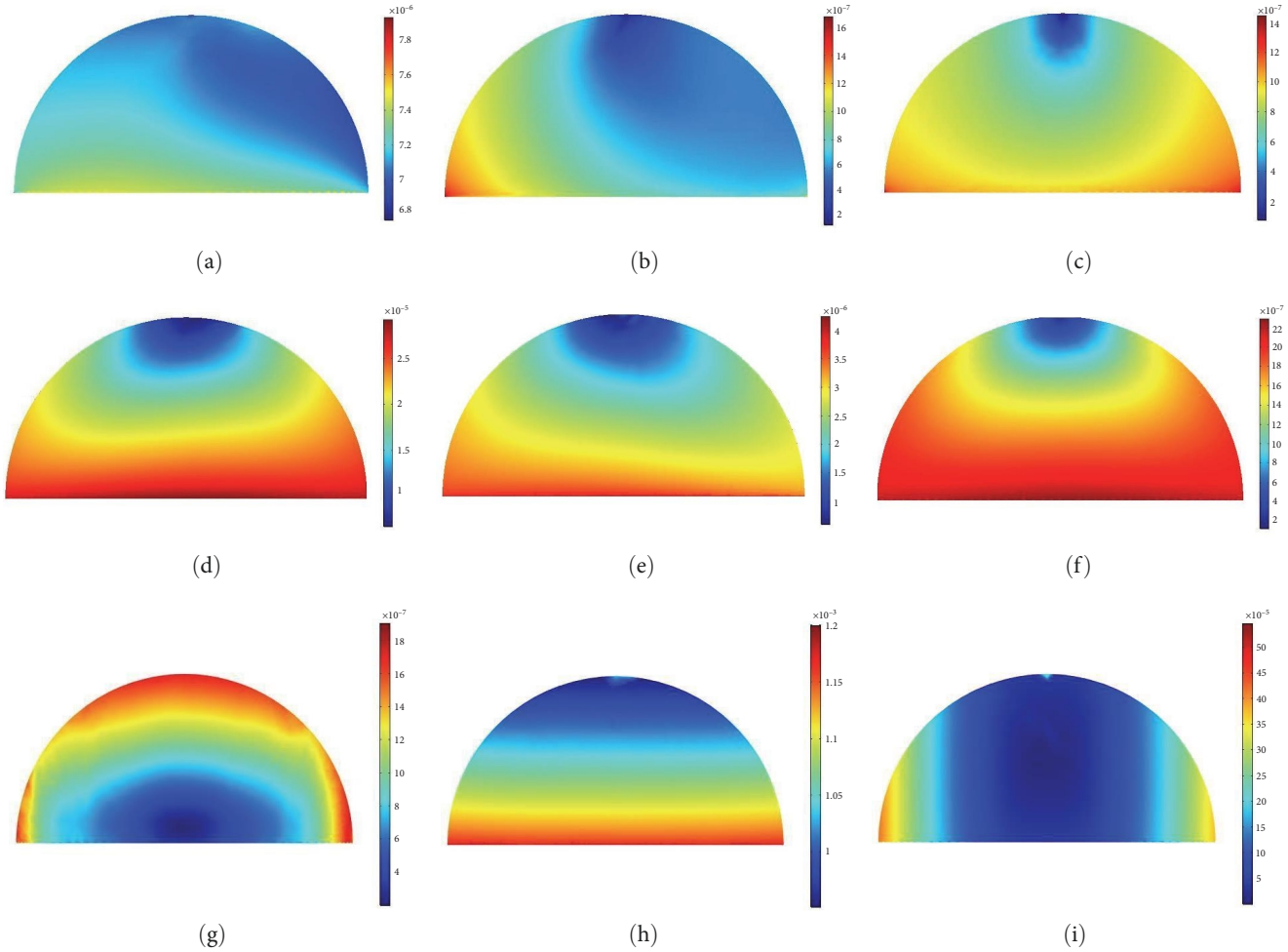

Figure 8: Load absorption at cracked point. (a) Position of crack at 0.01 m of iron beam. (b) Position of crack at 0.10 m of iron beam. (c) Uncracked iron beam. (d) Position of crack at 0.01 m of steel beam. (e) Position of crack at 0.10 m of steel beam. (f) Uncracked steel beam. (g) Position of crack at 0.01 m of titanium beam. (h) Position of crack at 0.10 m of titanium beam. (i) Uncracked titanium beam.

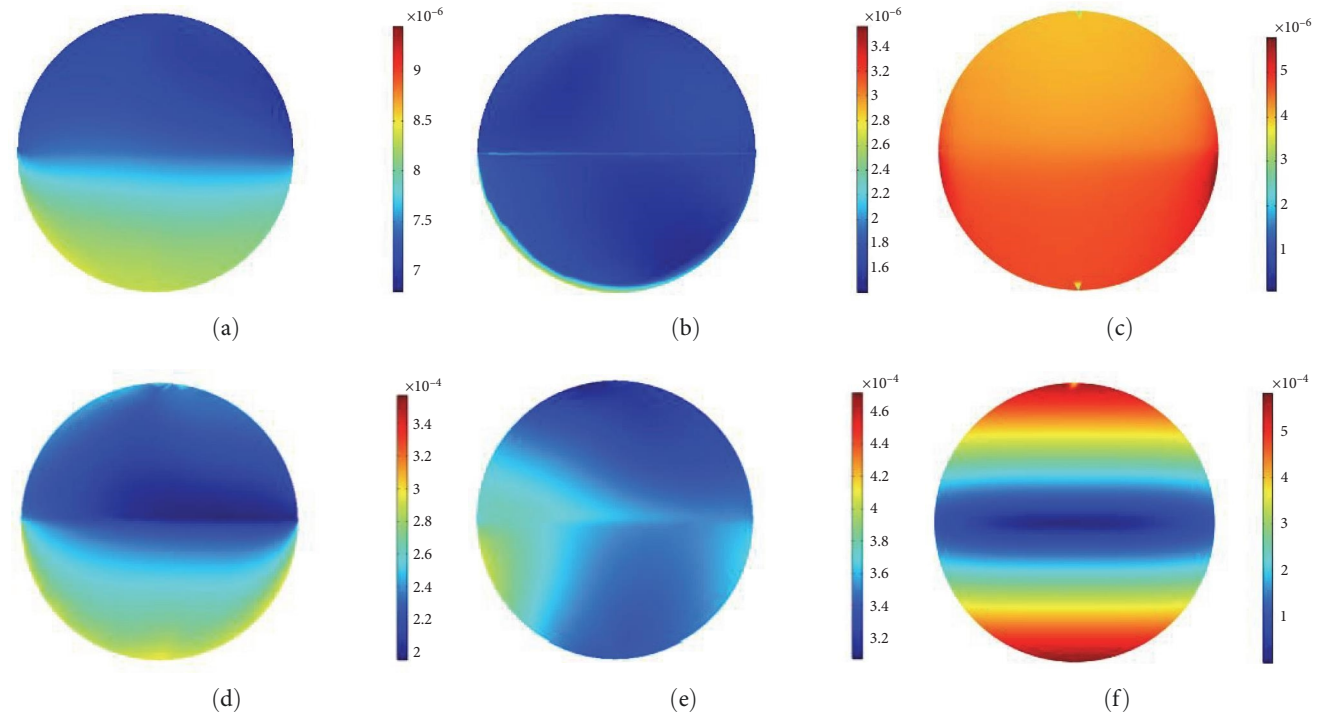

Figure 9: Continued.

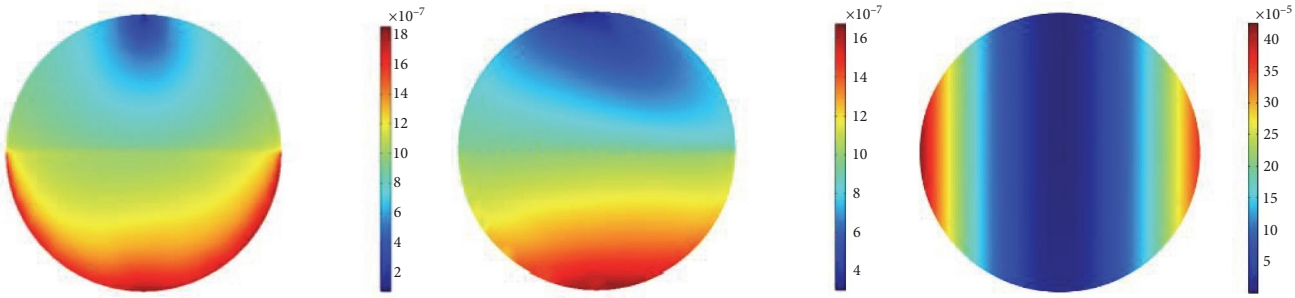

(g) (h) (i)

Figure 9: Cross-section of stress absorption at 0.0085 m and 0.085 m of cracked and uncracked beam. (a) Cross-section at 0.0085 m of cracked iron beam. (b) Cross-section at 0.0085 m of cracked steel beam. (c) Cross-section at 0.0085 m of cracked titanium beam. (d) Cross-section at 0.085 m of cracked iron beam. (e) Cross-section at 0.085 m of cracked steel beam. (f) Cross-section at 0.085 m of cracked titanium beam. (g) Cross-section at 0.0085 m of uncracked iron beam. (h) Cross-section at 0.0085 m of uncracked steel beam. (i) Cross-section at 0.0085 m of uncracked titanium beam.

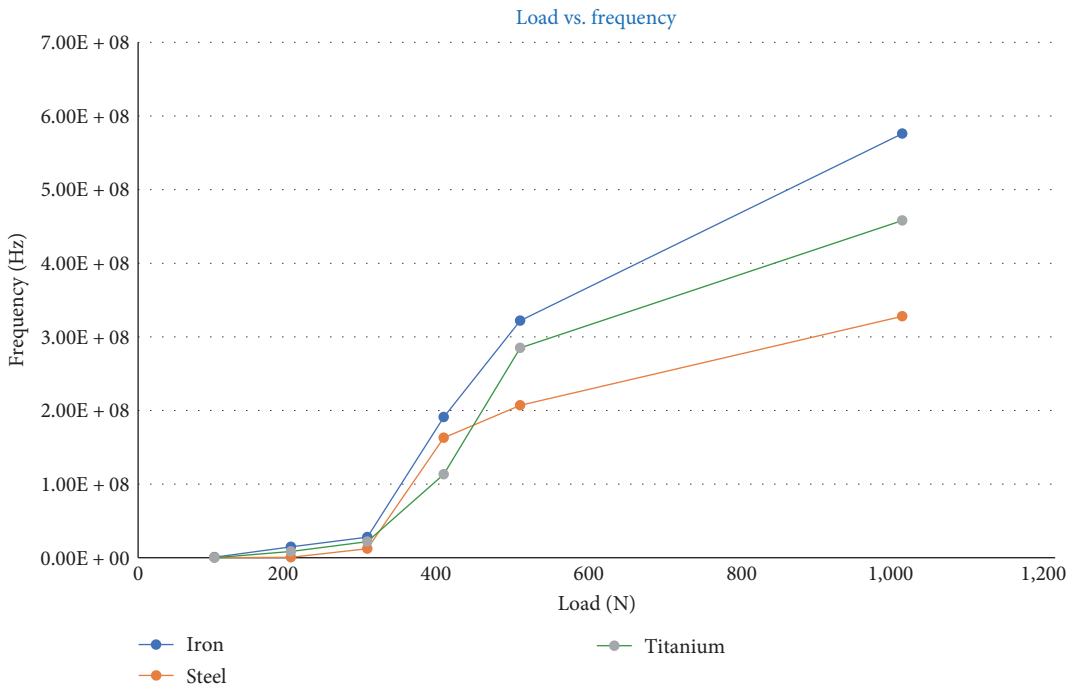

Figure 10: Frequency at fixed cracked position (at 0.10 m) of all beam for different load.

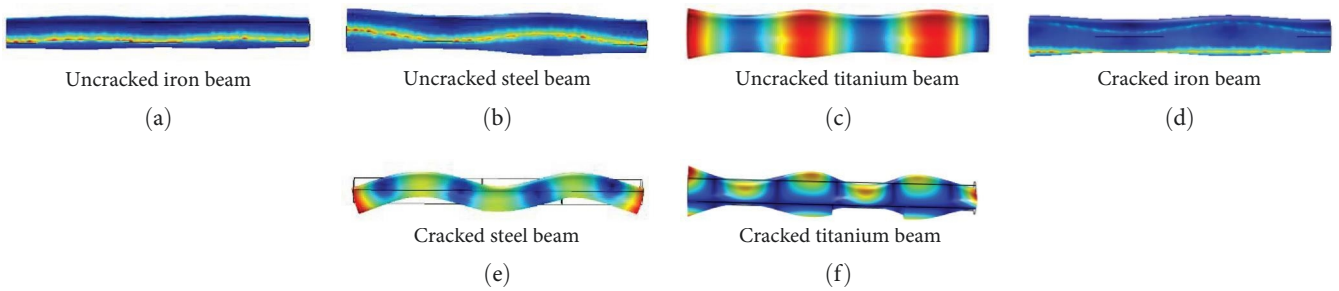

Figure 11: Deformation of computational domain after simulation. (a) Uncracked iron beam. (b) Uncracked steel beam (c) Uncracked titanium beam. (d) Cracked iron beam. (e) Cracked steel beam. (f) Cracked titanium beam.

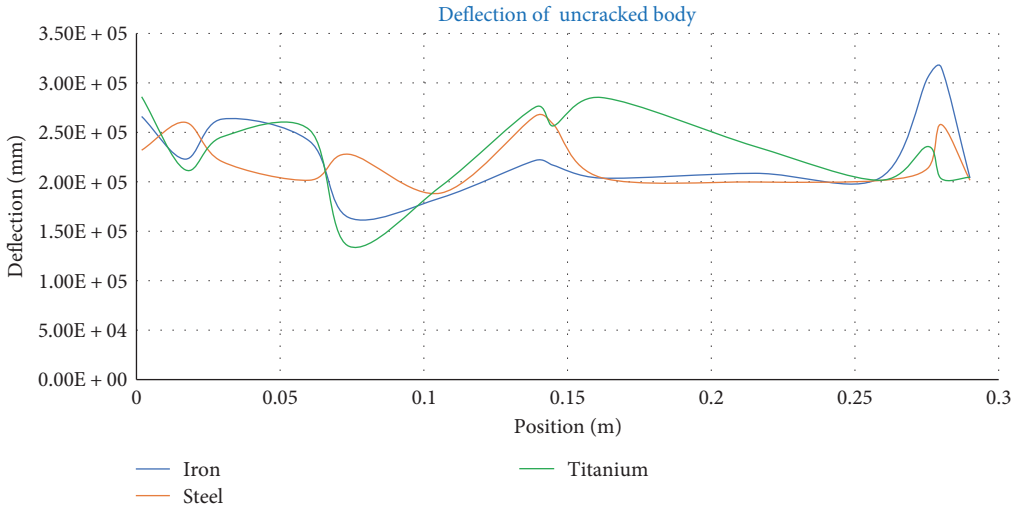

Figure 12: Deflection of uncracked iron, steel, and titanium body.

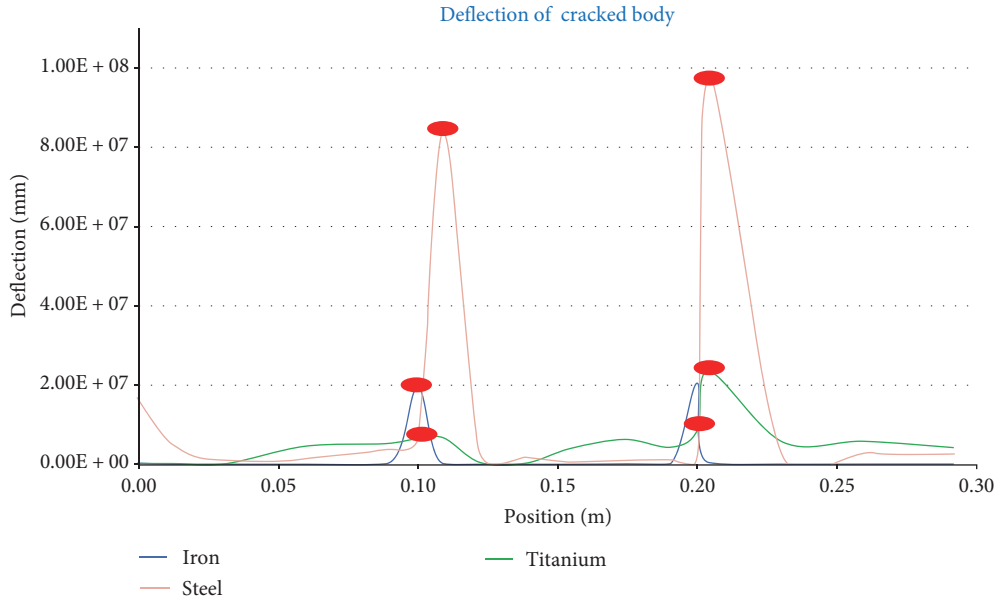

Figure 13: Deflection of cracked iron, steel, and titanium body.

monitoring by presenting the method for crack detection using vibration analysis.

Data Availability

All data used during the current study are available from the corresponding author upon request.

Conflicts of Interest

The authors declare that they have no conflicts of interest.

Acknowledgments

The authors would like to express their gratitude to the Centre of Excellence in Mathematics, Department of Mathematics, Mahidol University, Bangkok, Thailand, for their technical assistance. The authors would also like to thank the Simulation Lab, Department of Mathematics, Chittagong University of Engineering & Technology, Bangladesh, for their assistance in completing this study.

References

[1] I. A. Khan, A. Yadao, and D. R. Parhi, "Fault diagnosis of cracked cantilever composite beam by vibration measurement and RBFNN," *Journal of Mechanical Design and Vibration*, vol. 1, no. 1, pp. 1–4, 2013.

[2] E. V. V. Ramanamurthy and K. Chandrasekaran, "Vibration analysis on a composite beam to identify damage and damage severity using finite element method," *International Journal of Engineering Science and Technology*, vol. 3, no. 7, pp. 5865–5888, 2011.

[3] G. R. Irwin, "Analysis of stresses and strains near the end of a crack transverse in a plate," *Journal of Applied Mechanics*, vol. 24, pp. 361–364, 1956.
[4] R. Karmaker and U. K. Deb, "Effects of crack location and depths for an iron bar: a Finite Element approach," *Materials Today: Proceedings*, vol. 49, Part 5, pp. 2225–2233, 2022.
[5] D. P. Patil and S. K. Maiti, "Detection of multiple cracks using frequency measurements," *Engineering Fracture Mechanics*, vol. 70, no. 12, pp. 1553–1572, 2003.
[6] A. K. Darpe, K. Gupta, and A. Chawla, "Dynamics of a bowed rotor with a transverse surface crack," *Journal of Sound and Vibration*, vol. 296, no. 4-5, pp. 888–907, 2006.
[7] A. C. Chasalevris and C. A. Papadopoulos, "Identification of multiple cracks in beams under bending," *Mechanical Systems and Signal Processing*, vol. 20, no. 7, pp. 1631–1673, 2006.
[8] A. K. Darpe, "A novel way to detect transverse surface crack in a rotating shaft," *Journal of Sound and Vibration*, vol. 305, no. 1-2, pp. 151–171, 2007.
[9] M. S. Prabhakar, *Vibration analysis of cracked beam*, Thesis of Master of Technology on Machine Design and Analysis, National Institute of Technology, 2009.
[10] U. Dackermann, "*Vibration primarily based injury identification strategies for engineering structures victimisation artificial neural networks*," PhD Thesis, University of Technology, Sydney, 2010.
[11] S. K. Georgantzinos and N. K. Anifantis, "An insight into the breathing mechanism of a crack in a rotating shaft," *Journal of Sound and Vibration*, vol. 318, no. 1-2, pp. 279–295, 2008.
[12] S. Shahbazpanahi and A. Kamgar, "Fracture modelling of crack propagation in steel," *APCBEE Procedia*, vol. 9, pp. 197–201, 2014.
[13] I. Caliò, A. Greco, and D. D'Urso, "Structural models for the evaluation of eigen-properties in damaged spatial arches: a critical appraisal," *Archive of Applied Mechanics*, vol. 86, no. 11, pp. 1853–1867, 2016.
[14] M. Jirásek, "Damage and smeared crack models," in *Numerical Modeling of Concrete Cracking*, vol. 532 of *CISM International Centre for Mechanical Sciences*, pp. 1–49, Springer, Vienna, 2011.
[15] M. Cervera and M. Chiumenti, "Smeared crack approach: back to the original track," *International Journal for Numerical and Analytical Methods in Geomechanics*, vol. 30, no. 12, pp. 1173–1199, 2006.
[16] D. Kute and H. Mishra, "Two crack detection in tapered cantilever beam using natural frequency as basic criterion," *Global Journal of Engineering Science and Researches*, vol. 5, no. 7, pp. 228–233, 2018.
[17] R. P. B. Kocharla, R. K. Bandlam, and M. R. Kuchibotla, "Finite element modelling of a turbine blade to study the effect of multiple cracks using modal parameters," *Journal of Engineering Science and Technology*, vol. 11, no. 12, pp. 1758–1770, 2016.
[18] A. Kovalev, D. Kovalev, V. Panchenko, V. Kharchenko, and P. Vasant, "System of optimization of the combustion process of biogas for the biogas plant heat supply," in *Intelligent Computing and Optimization. ICO 2019*, vol. 1072 of *Advances in Intelligent Systems and Computing*, pp. 361–268, Springer, Cham, 2021.
[19] E. J. Hearn, "Strain energy," in *Mechanics of Materials 1 (Third Edition)*, pp. 254–296, Butterworth-Heinemann, 1997.
[20] R. Karmaker and U. K. Deb, "Crack detection of iron and steel bar using natural frequencies: a CFD approach," in *Intelligent Computing and Optimization. ICO 2020*, P. Vasant, I. Zelinka, and G. W. Weber, Eds., vol. 1324 of *Advances in Intelligent Systems and Computing*, pp. 224–236, Springer, Cham, 2021.
[21] COMSOL Multiphysics Software, https://www.comsol.com/product-download.
[22] J. Chen, E. Dörsam, J. Neumann, and S. Weißenseel, "Compressive stress–strain behavior of paper material affected by the actual contact area," *Journal of Print and Media Technology Research*, vol. 9, no. 1, pp. 7–19, 2020.